Acta of Bioengineering and Biomechanics
Vol. 24, No. 2, 2022

Original paper
DOI: 10.37190/ABB-02024-2022-03

sciendo

Novel curve fitting method based on constrained optimization for the modelling of human brain aneurysms using Mooney–Rivlin hyperelastic materials in the entire range of deformations til rupture

BRIGITTA K. TÓTH*, ANDRÁS LENGYEL

Department of Structural Mechanics, Budapest University of Technology and Economics, Budapest, Hungary.

Purpose: Brain aneurysms often prove fatal if ruptured, therefore, understanding their mechanical behaviour in the coupled system of vessels and blood flow can significantly help preventive surgical treatment. The purpose of this work was to analyse measurement data and to determine material parameters for the hyperelastic Mooney–Rivlin model for model building and numerical simulations of aneurysms. *Methods*: A total of 88 human brain aneurysm specimens of 41 patients obtained from surgery were processed in this work based on the tests performed by the authors in a previous project. A novel algorithm was proposed and applied in this work to fit stress–stretch ratio curves for multiple measurement data using constrained optimization with hard conditions to comply with known mechanical behaviour. *Results*: The method produced parameters of stretch ratio–stress curves for a number of groups of the specimens representing the average as well as the extreme stresses, separately for male and female subsamples. Stretch range both in compression and in tension up to rupture was covered and material stability for the entire range was also verified. *Conclusions*: The fitted curves with recommended range of validity are directly applicable to numerical finite element or coupled simulations of aneurysms supporting preventive medical treatment or decision making.

Key words: *aneurysm, internal carotid artery, Mooney–Rivlin model, curve fitting, material parameters, material stability*

1. Introduction

In recent years, several studies have addressed the formation and rupture of human brain aneurysms or pathological dilations of arteries [36], [38]. It has been in the focus of research both in medical and engineering sciences. From an engineering perspective, the problem is formulated as the two-way coupled numerical simulation [17] of the dilation evolved on the wall of the high deformation capacity elastic tube embedded in an elastic medium and the flow of the liquid inside and is the focus of many research activities [2], [24], [40]. Widening our knowledge on aneurysms and developing our modelling capabilities in numerical simulation can be beneficial from various aspects. Formation of aneurysm has not yet been fully explained up to present time. Though we have some knowledge on predisposing factors, predicting the probable locations of dilations on a healthy artery segment or the risk of rupture of an existing aneurysm would be of great service for medical science. It may also help in decision making in planning surgical treatments.

Software packages used by engineers for numerical simulations require the input of material parameters. Provided that tissue samples from past treatments of the patient involved are already obtained, model-

* Corresponding author: Brigitta K. Tóth, Budapest University of Technology and Economics, Műegyetem rkp. 3., Budapest, Hungary. Phone: +3614634044, e-mail: toth.brigitta@emk.bme.hu
Received: January 24th, 2022
Accepted for publication: May 4th, 2022

ling can be tailored to the patient's characteristics [5], [23], [46]. Unfortunately, it is very rare and, even if available, such data may bear little relevance to the material properties of the artery wall at other locations for various reasons, e.g., local plaques, structural lesions, variance in collagen fibre distribution, to mention a few. Consequently, the need arises to use group related characteristics as a database in the modelling in general cases.

It is well-known that material properties of biological tissues have large variance. In such cases, a major difficulty is that curve fitting to measured data is fully justifiable only for the range of the shortest data set of the sample. This approach was taken in Tóth's dissertation [41]. While it is reliable in the investigated interval, it cannot yield a realistic, physically feasible representation of the well-known shape published by Holzapfel et al. [11] over the entire range.

Histological structure of vessel walls is in correspondence with their physiological role, as it constantly varies along the arterial system from the large arteries through the arterioles as far as the smallest capillaries. Detailed analysis on various mechanical properties and general behaviour of blood vessel can be found in [33], [35] and for passive and active *in vitro* behaviour of arteries see [11], [14] as well as [25]. Mechanical analysis of any 'structure' requires a careful study of material behaviour since reliability of data processing strongly depends on the quality and extent of available experimental data, i.e., specimens. In the lack of appropriate *in vivo* tests, data can be obtained from *in vitro* tests with approximate boundary conditions imitating real physiological environment. Note that *in vivo* tests would be naturally favourable because they enable the analysis of vessels under real physiological conditions. The invasive ones are strongly limited due to their nature as well as ethical issues, however, non-invasive ones can also serve to gain information on, e.g., vessel wall stiffness [15], [16], [22]. Furthermore, mechanical tests can be directly performed on tissue samples *in vitro* to obtain data for the mechanical modelling. Since arterial tissues do not change their volume in the physiologically realistic range of deformations, they are considered as incompressible materials [11].

Although important information can be gained about the material from pulling tests on strips, understanding shear behaviour of artery walls would also be of significance under combined loading [30], [31]. However, this is beyond the scope of this study.

The unloaded state of the artery wall does not imply it being stress-free as the unloaded artery ring has self-stress [11]. *In vitro* tests cannot reproduce these conditions. Composition of layers of artery walls varies along the vascular system [11], though these stress–stretch ratio diagrams are essentially the same in character.

Another issue, which is necessary for understanding the normal and pathological behaviour of vessels but is also beyond our present scope, is the quantitative description of viscoelastic behaviour of arteries. Hudetz and Monos [18] created a visco-elastic model to simulate active mechanical reactions. Monos and Szűcs [26] processed experiments on passive and active biomechanical properties of isolated vessels taken from various samples (dog, pig, sheep, human) using instruments for cylindrical artery tubes. Tóth et al. [42], [43] determined visco-elastic properties of brain aneurysms.

Large deformation capability of artery walls is tackled by the application of hyperelastic constitutive models in numerical simulations, among which variants of the Mooney–Rivlin model [27], [34] are generally used for the description of rubber-like materials, though several others have also been proposed, e.g., 2D models by Vaishnav et al. [45], Fung et al. [9] or Takamizawa and Hayashi [37], 3D models by Chuong and Fung [4], Yeoh [47], Delfino [7], and a multilayer model by Holzapfel [11].

Prendergast et al. [32] performed uniaxial and biaxial test on five porcine aorta specimens and four human femoral artery specimens, fitted stress–stretch ratio curves using a special 9-parameter Mooney–Rivlin model by omitting some parameters. Yang et al. [46] measured axial and circumferential stress–stretch ratio data of one cadaveric human coronary plaque specimen and computed fitted curve using a modified Mooney–Rivlin model with exponential terms. Arterial wall properties for the 2-parameter Mooney–Rivlin model were calculated in [6]. One alternative approach to the analysis of deformations of arteries is to apply internal pressure and axial load to artery segments with closed ends [12]. Modelling of artery walls incorporating the layers was discussed by Holzapfel and Weizsäcker [14] and Holzapfel [10], using Fung-type strain energy function for the description of the orthotropic contribution to the complex model in addition to the isotropic ground matrix. Holzapfel et al. [13] performed uniaxial tensile tests on strips taken from the three layers of coronary arteries obtained from thirteen human cadavers. Tests included cyclic loading in the physiologically realistic range of deformations, and ultimate stretch ratios and stresses were also determined. They calculated material parameters for their previously proposed strain energy function individually for each specimen. Noble et al. [29] used

inverse finite element modelling to determine material parameters of neo-Hookean and linear elastic constitutive models for ten human cadaveric femoral artery specimens with plaque based on experiments during which several pressure levels were applied while recording intravascular ultrasound and virtual histology imaging. Cosentino et al. [5] performed biaxial tests on ascending thoracic aortic aneurysms obtained via surgery from nine patients and determined patient-specific material properties for Yeoh and Fung constitutive models.

As is apparent from the literature, in most cases, animal samples are used and whenever human samples are available, the vast majority are cadaveric. Tissue samples from aneurysms are exceptionally rare as they are acquired through surgery. Further difficulties are posed by the fact that aneurysms are artery dilations, often at bifurcations, thus it is hard or even impossible to determine specimen orientation with respect to the parent artery cardinal directions after extraction.

In this work we process uniaxial measurement data based on the previous work by the first author, reported in [41]. We had at our disposal stress–stretch ratio curves of uniaxial tests on human brain aneurysms extracted during surgery, partially evaluated focusing only on the initial range of the data at that time. The present study aims to reconsider the measurement data in order to fit curves over the largest possible range of the stretch ratio with the intention of providing material constants for numerical simulations of artery walls not only in the initial range but also up to potential aneurysm rupture, also expecting stress–stretch ratio curves to comply with the general shape presented by Holzapfel et al. [11]. Tóth [41] found significant differences with respect to sex in the measurement data, therefore male and female specimens are to be processed separately. The 5-parameter variant of Mooney–Rivlin model is chosen as it is incorporated in various finite element software packages and is sufficiently sophisticated to approximate observed characteristics of stress–stretch ratio curves.

The objectives of this study were as follows. First, in order to fit curves for large domains of stress–stretch ratio data, a new approach is necessary. We proposed a method which is a combination of a constrained optimization problem using energy and stress-based conditions and an extension of linear regression for curve fitting based on the sum of squared residuals. As patient specific data are in most cases impossible to acquire, simulations have to use model parameters that represent realistic material behaviour of a group of specimens selected with respect to certain factors, e.g., sex, age, etc. Even though biological tissues may exhibit large deviations, such group related parameters are necessary for the modelling. Therefore, secondly, this algorithm was applied for several different problem formulations. The primary aim was to fit curves separately for male and female subsamples but within the groups curve fittings are proposed to represent the average (general) behaviour as well as the extreme low and high performance in terms of stresses. It was an important objective of our analysis to obtain curves which are both optimal solutions and represent realistic materials. As a result of the proposed method, material parameters for the Mooney–Rivlin model are calculated.

The outline of the paper is as follows. Section 2 briefly describes the tests reported earlier by Tóth [41] and elaborates the proposed method to fit stress–stretch ratio curves corresponding to the Mooney–Rivlin hyperelastic model to the measured data. Section 3 summarizes the results and evaluation is discussed in Section 4. Section 5 gives concise conclusions.

2. Materials and methods

2.1. Tests

Measurements on the walls of aneurysms were conducted at the Institute of Human Physiology and Clinical Experimental Research of the Semmelweis University, Hungary, in which the first author was a collaborator [41]. Stripes were cut out of the aneurysm in internal carotid artery for the uniaxial tests. Stress–stretch curves for a total of 88 valid specimens were measured and recorded. The specimens were categorized with respect to whether they belonged to male or female patients. Wherever it was possible, the orientation of the specimen (i.e., meridional or circumferential) was also identified with respect to the approximately spherical shape of the aneurysm itself but no reliable relationship could be established with the standard notion of axial or circumferential directions of ordinary cylindrical artery walls. Statistically significant differences in orientation were not found (which is in correspondence with findings on abdominal aortic aneurysms [20]). Several factors were also considered, some contained in PHASES score (hypertension, age, size of aneurysm, earlier SAH, site of aneurysm) and others (status (ruptured/unruptured), presence of other aneurysms with status, etc), how-

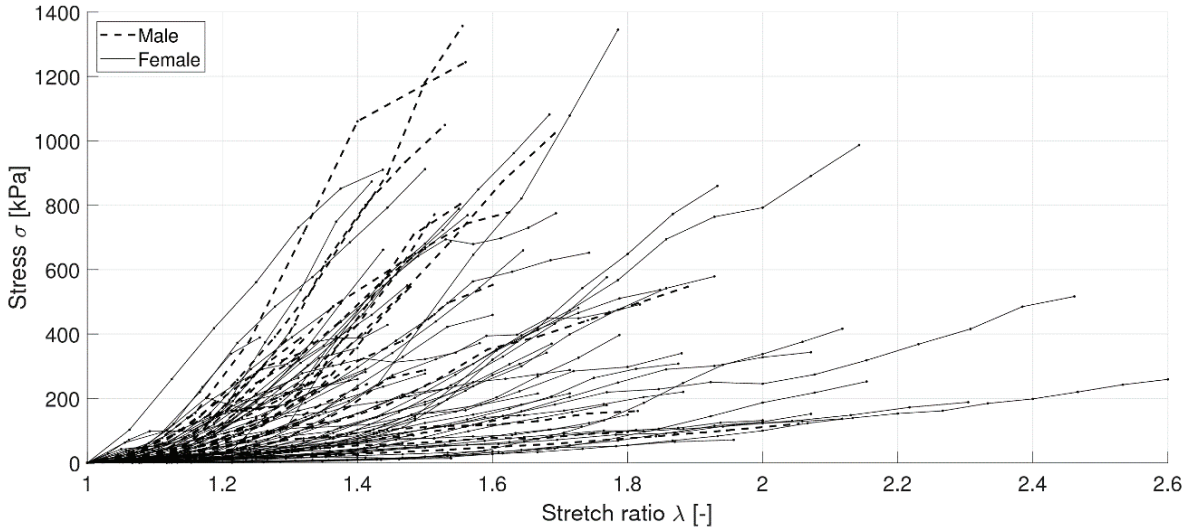

Fig. 1. Stress–stretch ratio measurement data from uniaxial tests on aneurysms

ever, the sample was not large enough for statistics on pathological history. In terms of age, division at the age of 70 as in PHASES leaves a very limited sample above it, mostly female specimens, and setting other age groups requires preliminary statistics to justify the categorization. In terms of aneurysm status, we faced the problem of handling additional possible aneurysm in the patient with its status leading to some combination of cases. Altogether, to illustrate the application of the proposed method, categorization of the sample was made only with respect to sex in this study. Stress–stretch ratio curves for all specimens are plotted in Fig. 1. Specimens from male and female patients are distinguished and plotted in dashed and solid lines, respectively.

Male specimens are typically characterized by less deformation capacity but higher strength and stiffness than the female ones. The ultimate stretch ratios and stresses (i.e., end point of each curve) are scattered in a large domain. In the male and female subgroups, the mean of ultimate stretch ratio is 1.547 and 1.685, respectively, and the mean of ultimate stress is 515.3 kPa and 407.9 kPa, respectively. Owing to the significant differences between the two subgroups, they have been analysed separately.

2.2. Method

2.2.1. Mooney–Rivlin material model

For material modelling of arterial walls, the Holzapfel–Gasser–Ogden model (HGO) [11] can be a good candidate because it is suitable for fibre-reinforced composite materials. However, we had no samples for the measuring of fibre direction vectors, as well as we did not aim for the modelling of the complex structure in the scale of its constituents but rather globally. Therefore, the Mooney–Rivlin [27], [34] model was chosen in our analysis because it is applicable to several hyperelastic rubber-like materials (i.e., with large deformation capacity) and is implemented in most finite element software packages. There are types with 2, 3, 5, or 9 parameters. As the number of parameters increases, more complex behaviour can be modelled, that is for single, double and triple curvature solutions 2 or 3 parameters, 5 parameters and 9 parameters can be used, respectively. We have opted for the 5-parameter type to achieve the expected shape in [11] with a possible double curvature, whereas the 9-parameter type may be too unstable to fit well-defined curves. The model formulates the deformation energy function in terms of the invariants as

$$\Psi = c_{10}(I_1' - 3) + c_{01}(I_2' - 3) + c_{20}(I_1' - 3)^2 + c_{11}(I_1' - 3)(I_2' - 3) + c_{02}(I_2' - 3)^2, \quad (1)$$

where I_1' and I_2' are the first and second deviatoric strain invariants, respectively, and parameters c_{10}, c_{01}, c_{20}, c_{11} and c_{02} define deviatoric deformations of the material. The invariants can be expressed in terms of stretch ratio λ. The Cauchy stresses in terms of λ, as derived in [41], can also be given with the above coefficients. Our goal was to determine such coefficients c_k ($k \in \mathbf{K} = \{10, 01, 20, 11, 02\}$) that the best representation of the measurement sample were obtained. For this purpose, the case of a single data set (i.e., a single stress–stretch ratio diagram) was solved first and then generalized for the case of fitting to multiple data.

2.2.2. Fitting curves to single data set

A schematic diagram of a measurement data set is shown in Fig. 2a. Dots represent data points (λ_i, σ_i) of the measured stress–stretch ratio function $\sigma(\lambda)$, which is assumed piecewise linear in the numerical computations. The approximation of the data is represented by function S expressed in terms of the base functions $S_k(\lambda)$ and parameters c_k:

$$S(\lambda;\mathbf{c}) = \Sigma_k c_k S_k(\lambda)\,, \tag{2}$$

where the base functions are obtained from Eq. (1) by differentiation [41]:

$$\begin{aligned} S_{10} &= 2(\lambda^2 - \lambda^{-1}), \quad S_{01} = 2(\lambda - \lambda^{-2}),\\ S_{20} &= 4(\lambda^4 - 3\lambda^2 + \lambda - 2\lambda^{-2} + 3\lambda^{-1}),\\ S_{11} &= 6(\lambda^3 - \lambda^2 - \lambda - \lambda^{-3} + \lambda^{-1}),\\ S_{02} &= 4(2\lambda^2 - 3\lambda - \lambda^{-4} + 32\lambda^{-2} - \lambda^{-1}). \end{aligned} \tag{3}$$

The evaluation of any approximation is based on the method of least squares, but instead of calculations of discrete points, we defined an error function representing the sum of squares of the differences between the simulated and the measured functions expressed as an integral over the interval (λ_1, λ_N):

$$f(\mathbf{c}) = \int_{\lambda_1}^{\lambda_N} (S(\lambda;\mathbf{c}) - \sigma(\lambda))^2 \,\mathrm{d}\lambda\,. \tag{4}$$

The optimal approximation minimizes the error function in terms of the parameters c_k, therefore the partial first derivatives must vanish: $\partial f(\mathbf{c})/\partial c_k = 0$. Since S is linear in the coefficients, this leads to a linear equation system $\mathbf{Ac} = \mathbf{b}$, where

$$\begin{aligned} a_{jk} &= \int_{\lambda_1}^{\lambda_N} S_j(\lambda) S_k(\lambda)\mathrm{d}\lambda,\\ b_k &= \int_{\lambda_1}^{\lambda_N} S_k(\lambda)\sigma(\lambda)\mathrm{d}\lambda, \quad j,k \in \mathbf{K}, \end{aligned} \tag{5}$$

from where parameters c_k and then the simulated function S can be computed using Eq. (2).

2.2.3. Fitting curves to multiple data sets

In order to create curves representing a selection of specimens in the sample, the fitting based on the sum of squared residuals must be extended to contain multiple data sets, as shown by a schematic diagram in Fig. 2b. The task is to fit a single curve to all data sets that provides the best representation of the data in the selection. It should be taken into consideration that each data set

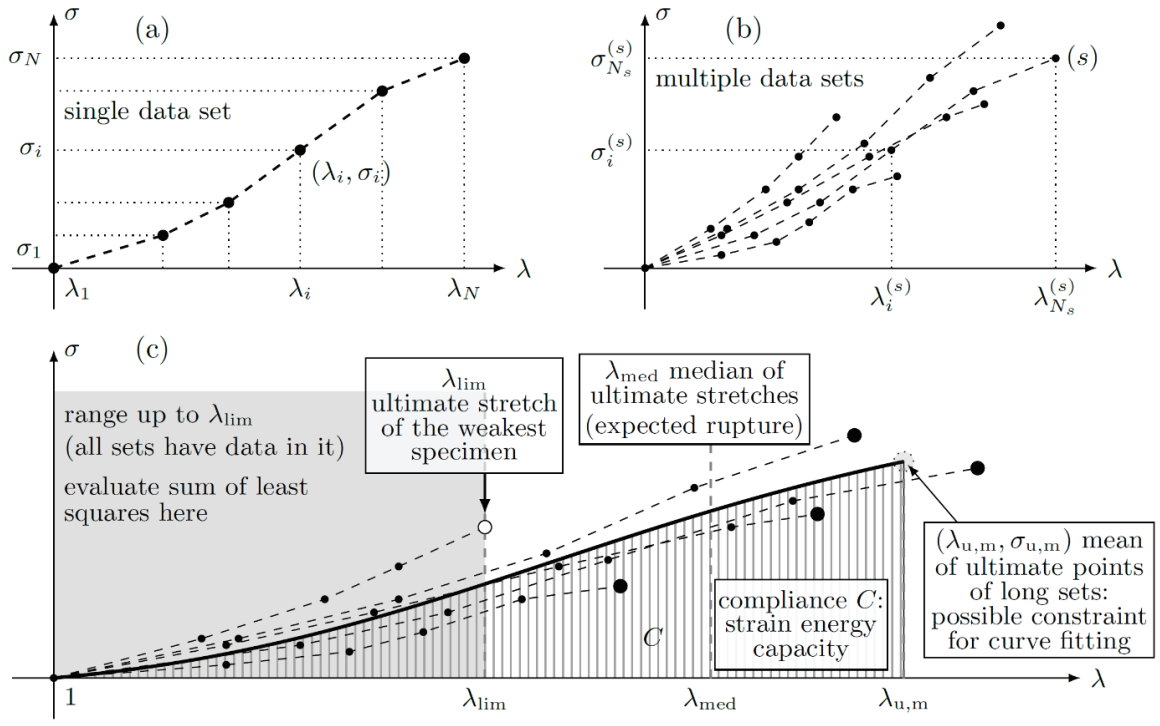

Fig. 2. (a) Schematic plot of measurement data on stress–stretch ratio relationship for a single data set, (b) Schematic plot of multiple measurement data for stress–stretch curves, (c) Scheme of curve fitting to multiple measurement data. Dashed lines with dots denote measurement data, among which large filled dots show the end points of curves, the solid thick curve represents the simulated curve, the shaded area indicates the range of λ for which the sum of squares is computed and the area highlighted with vertical lines represents the compliance of the simulated curve. Interpretation of the limit, median, and the mean of the ultimate points is also displayed

may have different number of points at different abscissa values, and that the maximum abscissas are also different. Note that the sample may possibly be divided into groups with respect to various factors since the specimens originate from individuals of different sex, age, or health conditions, etc., therefore, curve fitting tasks can also be defined for various selections of specimens or the entire sample, too. The particular problems investigated in this study are presented in Section 2.3.

The minimum of the ultimate deformations of the specimens, i.e., the end of the shortest data set defines an upper limit λ_{lim}, below which all specimens contain measured stress values and above it they terminate one by one at different λ values. Consequently, the application of the method of least squares is only justified in interval (1, λ_{lim}), where all data sets are equally represented. Beyond that limit, the shape of the fitted curve is not controlled, therefore, we propose an approach combining the error function with suitable boundary conditions based on certain statistical properties of the entire range of curves. The fitted curves then can represent the mechanical behaviour of the sample also in the range beyond the common interval. The approach is illustrated in Fig. 2c. In the diagram, the gray shaded area highlights the range of stretch ratio (up to λ_{lim}, the end point of the shortest data set) where the evaluation of sum of squares is justified. To determine the curve for the rest of the domain, certain conditions must be introduced, which may refer to the stresses or other mechanical properties. For example, the area with vertical lines represents the compliance C, the strain energy capacity of fitted curve, which can be prescribed to equal the mean compliance of the sample. Also, one may require the solution to fit to particular points, e.g., point ($\lambda_{\text{u;m}}$, $\sigma_{\text{u;m}}$) indicated by a gray circle, which represents the mean of the ultimate stress at the mean ultimate stretch ratio of some selected specimens, or similarly a point defined at the median of the ultimate stretch ratios, indicated in the diagram as well (the median has the significance of giving an estimate on the expected stretch at rupture). It is also possible to set constraints on the slope (first derivative) or the inflexion (second derivative) of the curve. The choice of conditions need to be considered individually in each curve fitting task. The specifics of each case are shown in Section 2.3.

The total sum of squares $f(\mathbf{c})$ for the whole data in range (1, λ_{lim}) is computed as the sum of individual sums given in Eq. (4) with upper limit of integration set to λ_{lim}. The function and its derivatives are elaborated in the same way as for the single curve fitting, and coefficients are formulated as in Eq. (5).

Boundary conditions may refer to the value of stress or its derivatives at the ultimate stretch ratio of the curve, or the compliance. If the value of a quantity, e.g., the stress, evaluated at any particular λ_0 is expected to be in an interval, then two inequality constraints are defined as $g_1(\mathbf{c}) = S(\lambda_0; \mathbf{c}) - \sigma_{\text{low}} \geq 0$ and $g_2(\mathbf{c}) = -S(\lambda_0; \mathbf{c}) - \sigma_{\text{high}} \geq 0$. If conditions for the compliance C or for the derivatives of the stress are required, then they are expressed with the base functions and then similar conditions are formulated. If hard conditions are formulated for a quantity to take a specific value, then the respective inequality is replaced with an equality constraint. Soft conditions with penalization are not included in this analysis.

The minimization problem with several inequality constraints formally reads as

$$P_{\text{constr}} = \begin{cases} \text{minimize} & f(\mathbf{c}), \\ \text{subjected to} & \mathbf{g}(\mathbf{c}) \geq 0, \end{cases} \tag{6}$$

based on the well-known Karush–Kuhn–Tucker optimality conditions [19], [21] (for a recent source see [1]), where $\mathbf{g}(\mathbf{c})$ is a vector of algebraic expressions in the design variables $\mathbf{c}$. The solution is approached through the Lagrangian $\mathcal{L}(\mathbf{c}; \boldsymbol{\mu}) = f(\mathbf{c}) - \boldsymbol{\mu}^{\text{T}}\mathbf{g}(\mathbf{c})$, where vector $\boldsymbol{\mu}$ contains the multipliers μ_j (j = 1, ...). At the minimum all of the partial first derivatives with respect to the variables (including the multipliers) should vanish: $\partial\mathcal{L}/\partial c_j = 0$ and $\partial\mathcal{L}/\partial\mu_j = 0$. Since the boundary conditions are linear in $\mathbf{c}$ and the Lagrangian is also linear in the multipliers, a linear equation system is obtained.

The solution of the equation system yields the parameters c_j and multipliers μ_j. Each constraint is active at the optimum if the respective multiplier is non-negative, and in this case the inequality is equivalent to an equality. If some of the constraints are inactive, a new problem formulation is required in which the inactive constraints are omitted.

2.3. Application for curve fitting

2.3.1. General considerations

In this section, the problem formulation and boundary conditions are given for all cases of curve fitting together with the numerical results. As stated in the Introduction, the aim of this analysis is to determine the parameters of fitted curves for numerical modelling of aneurysms in order to support decision making in medical treatment of patients. As patient specific

data are not possible to obtain, only samples from past surgeries (Fig. 1) can be used to produce statistical representations of several specimens in the modelling. The sample is diverse so it is expedient to distinguish specimens with respect to certain factors and fit curves for a few selections. Primarily, subgroups of male and female specimens are analysed separately. We have not found publications on the distinction between sexes because most measurements involved samples of smaller scale, though such a study was done on rats [28]. The graphical representation highlights that the female specimens are generally softer, i.e., typically having lower secant modulus and larger ultimate stretch ratios, as verified by our calculations. We have found that the samples followed normal distribution with equal variances, and after performing two-sample *t*-tests, found difference between the sexes at statistical significance level $p = 0.05$. In both subgroups, three cases are solved: curve fitting to the entire sample, to the high strength specimens and to the low strength specimens, in order to represent the hypothetical 'average' patient, as well as the stiff and the soft material behaviour, respectively, and also to capture the general character of the measured data.

Each of these calculations requires curve fitting to selection of data sets according to Section 2.2.3, involving the minimization of the error function and application of suitable constraints. A number of considerations have to be made in all cases as follows. First, the error function can only be formulated for the common abscissa interval $(1, \lambda_{\text{lim}})$ of the selected specimens, which depends on the selection and constitutes a fraction of the range of the individual specimens. Constraints need to be applied to determine the shape of the curve beyond the initial common interval. They are not only arithmetic representations of the numerical data but are expected to comply with the observed character of the mechanical behaviour. The latter one cannot be formulated with mathematical rigor and exactness, consider, e.g., monotonicity in various points or the alternation of softening and hardening phases of the observed mechanical behaviour. As five parameters are to be defined, a maximum of five constraints can be exactly satisfied. Therefore, the aim is to capture key numerical values or shape characteristics (e.g., inflexion or slope) with the constraints that result in fitted curves that are verified to comply with the observations. These constraints may vary from case to case.

Second, the representations of the extremes of the sample (based on a selection of extreme specimens) have possibly limited abscissa range compared to the entire sample. They are not identical but very close to what one may call the lower and upper envelopes of the data, therefore we shall refer to them as quasi-envelopes.

Third, large variations, i.e., large relative standard deviations are characteristics of samples of organic (human) specimens. It is observed in the case of ultimate stretch ratio, ultimate stress, as well as compliance. However, we also note that the mean compliances of the male and the female subgroups are very close to each other, being 111.6 kPa and 104.4 kPa, respectively. Using a two-sample *t*-test, the compliance of the male and the female samples are not independent (i.e., the test rejects the null hypothesis on independence) at a very high significance level of $p = 0.734$. This suggests that the compliance may play a significant role in the elastic behaviour of such tissues, therefore we rely on compliance as a mechanical property for the fitting of the curves whenever possible, further to fitting to specific values in the stress–stretch ratio diagram, etc.

Fourth, the Mooney–Rivlin model represents real material behaviour only if it satisfies the Drucker stability condition $\mathrm{d}\sigma_{ij}\mathrm{d}\varepsilon_{ij} \geq 0$, i.e., the incremental internal energy can only increase. For a one-dimensional problem, it is equivalent to have a monotonously increasing stress–stretch ratio curve. One may also consider the task in context of the more general concept of thermodynamic feasibility of hyperelastic materials formulated by the T-C inequalities [44] based on the Helmholtz free energy. It follows from it that it demands the vanishing of the first derivative of the deformation energy and the positiveness of the second, which, in fact, are automatically satisfied by the monotonicity mentioned above (it is shown in the following sections that monotonicity in each investigated case was achieved). To have a non-negative slope at the start, $c_{10} + c_{01} \geq 0$ must hold as obtained from the first derivative of the function (2) evaluated at $\lambda = 1$. For any other point, the check can be performed once the solution is computed. If the check fails, conditions are necessary. As negative slopes imply the presence of inflexions, the objective also can possibly be achieved by enforcing inflexion at certain points of the curve.

Fifth, it may also be important to extend the applicability of fitted curves to compression ($0 < \lambda < 1$). Although the tests are performed in the tensile range, contraction also occurs in tissues, therefore it is reasonable to prescribe material stability for part of the compression range. Lower limit $\lambda = 0$ corresponds to the physically unattainable state of infinitely compressed material. As the ultimate measured stretch ratio is ca. 2.6, the corresponding lateral contraction

of an incompressible material is $1/\sqrt{\lambda} \approx 0.62$. Also, due to possible additional compressive effects, we wish to create stable curves from $\lambda = 0.4$. This extreme value is unlikely to be present in large domains of a finite element model, however, since it may occur locally, the definition of such stable material models can avoid numerical instability of a simulation. The stress–stretch ratio curves are to be hardening in the compression range as approaching $\lambda = 0$ would imply the magnitude of stress increasing to negative infinity. The initial part of the tension range is also expected to be hardening, as mentioned previously, resulting in a shape of an odd function locally at $\lambda = 1$. It can be easily achieved by enforcing inflexion at this point.

2.3.2. Male specimens

Twenty-three specimens of the sample belonged to male patients with ultimate stress ranging between approx. 100 kPa and 1350 kPa, and ultimate stretch ratio ranging between approx. 1.25 and 2.05 with mean value 1.547 (Fig. 1).

The upper region contains three data sets, visibly separated from the others, therefore we define the upper quasi-envelope of the sample as a curve fitted to these sets according to the procedure elaborated in Subsection 2.2.3, Fig. 3a. The common part of the sets ends where the shortest one terminates (label "limit" in the diagram), thus the error function is formulated for this domain. The unconstrained solution (dotted line) has a concave end section and also an initial concave section followed by an inflexion contradicting the observed mechanical behaviour [11], therefore a new curve is proposed and formulated by adding a few constraints. One of them is to fit the curve to the mean of ultimate stresses at the mean of the ultimate stretch ratio (label "mean" in the figure), the second one eliminates the alternating convex and concave sections by enforcing inflexion in the origin, and it is also possible to prescribe the compliance (i.e., the deformation energy capacity) of the solution to equal the mean of the sample. The constrained solution (solid lines) is conform with mechanical expectations. It is found that the compression range is also hardening according to our expectations. (Note that the compression ranges are plotted in the summarizing figures in the Discussion.) The constrained solution constitutes the upper quasi-envelope of the male sample representing a compliance of 272.4 kPa, which is naturally larger than the mean of the entire male sample but considering the correctness of the obtained shape, the solution can be regarded reliable in the plotted interval.

In the lower region of the data, a single data set can be distinguished to define the minimum quasi-envelope, Fig. 3b. The error function is formulated according to Section 2.2.2. The unconstrained curve (dotted line) now also has a short initial slightly concave section, therefore, in the constrained optimization again constraints for the inflexion at the origin and for the compliance are formulated, but the fitting at the end point is unnecessary. The curve is in accordance with the expectation in the tension range but not hardening in compression. This problem is overcome by a third constraint enforcing inflexion at the end of the compression range (at stretch ratio 0.4). The constrained solution is shown in solid lines. Although it is computed using a single data set, it is in good correspondence with the general character of most of the specimens of similar strength and is hardening in compression. Its compliance is smaller than the mean compliance of the sample indicating that the curve might be adequate for a longer range.

Finally, curves are fitted to the data to represent the entire sample of male specimens, Fig. 4a. The common interval is very short in this case (label "limit"), and,

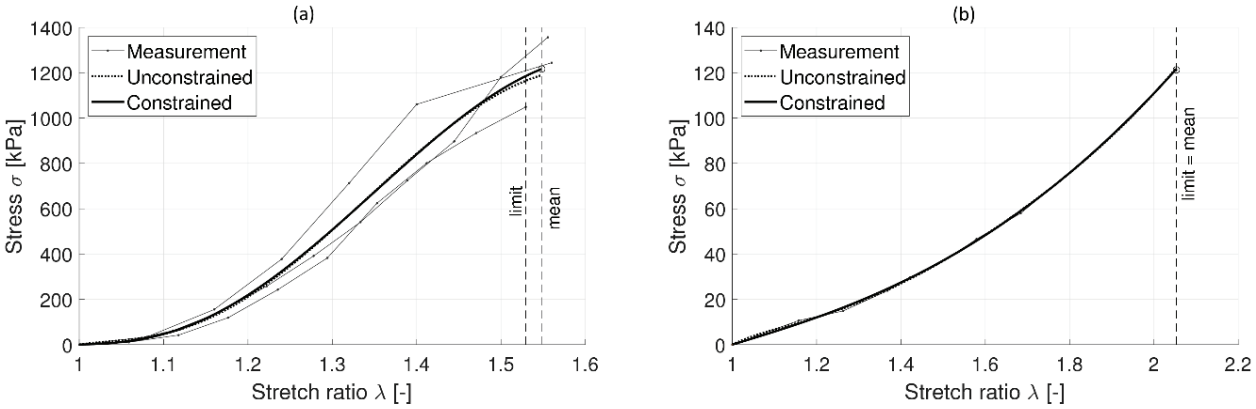

Fig. 3. Quasi-envelope curves for male specimens: maximum (a) and minimum (b); measurements are plotted in thin lines with dot markers, unconstrained and constrained solutions are plotted in thick dotted and solid lines, respectively

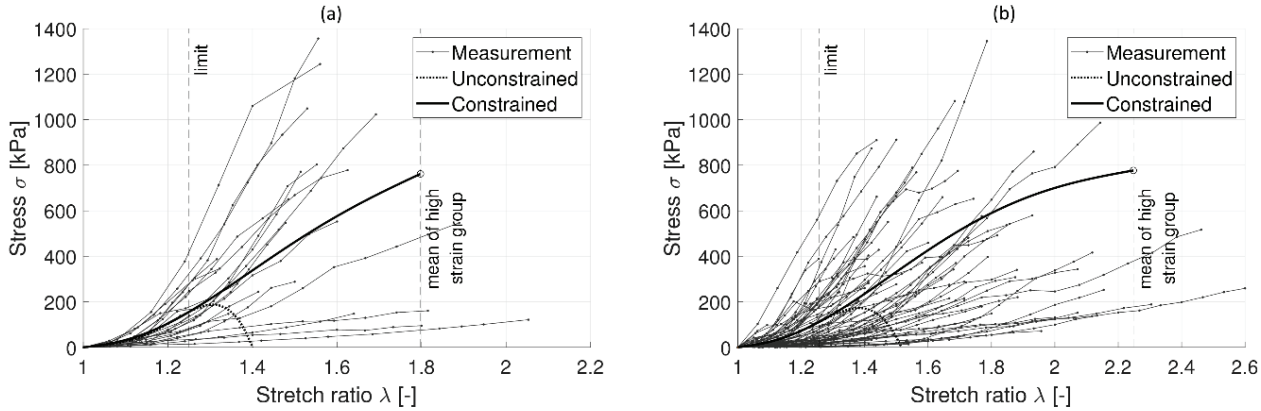

Fig. 4. (a) Curve fitting to all male specimens (a) and all female specimens (b); measurements are plotted in thin lines with dot markers, unconstrained and constrained solutions are plotted in thick dotted and solid lines, respectively

therefore, the unconstrained solution (dotted line) is ill-determined in the range beyond dropping below zero (which is obviously unfeasible mechanically). Constraints for the constrained optimization need to be chosen carefully because of fitting in a very large interval for widely scattering data. Realistic shape without alternating curvature or decreasing slopes could be achieved by the following conditions. As the unconstrained solution is regarded robust up to the limit, the constrained one should match its value at the limit as well as its start slope. The end point of the curve is now fitted to the mean of the four most outstanding curves ("high strain group" in the diagram) instead of the entire sample, and the wavy shape with ill-positioned inflexions are overcome by enforcing zero second derivatives at the start and at the end. The constrained solution (solid line) shows a realistic behaviour in the entire range and found to be stable in the compression range, too. The compliance of the curve measured up to the mean ultimate stretch ratio of all data sets is 114.03 kPa, almost equal to the mean compliance of the sample.

2.3.3. Female specimens

Sixty-five specimens of the sample belong to female patients. The ultimate stretch ratio had a mean value of 1.685, and a maximum of approx. 2.60.

Three high-stiffness specimens with similar slope, ultimate stretch and ultimate stress are located in the top left region of the diagram, and are, therefore, used for the maximum quasi-envelope (Fig. 5a). The unconstrained solution fitted to the common interval (label "limit") is plotted in dotted line. Note that it is only a good representation in that interval but starts decreasing beyond, thus, it is not a feasible stable solution. For the constrained solution, the curve is fitted to the mean of the ultimate stresses at the mean of the ultimate stretch ratio (label "mean") as well as the match for the mean compliance is also prescribed. To ensure applicability in a longer interval, fitting to the end point of another specimen with the absolute highest ultimate stress (Fig. 5a) is included in the constraints (label "extreme"). To avoid instability in the compression range and wavy shape, zero second de-

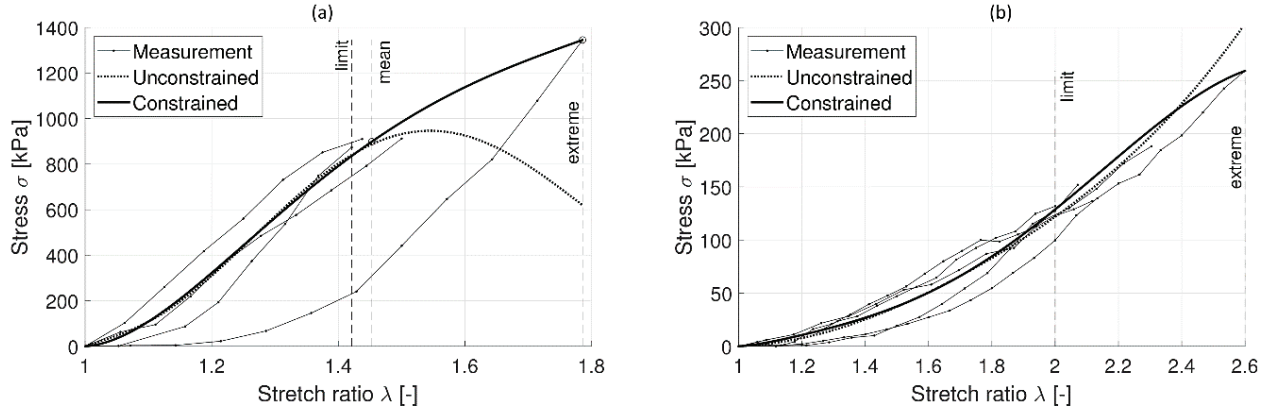

Fig. 5. Quasi-envelope curves for female specimens: maximum (a) and minimum (b); measurements are plotted in thin lines with dot markers, unconstrained and constrained solutions are plotted in thick dotted and solid lines, respectively

rivatives are enforced at the start and at the end of the curve. The solution (solid thick line) is in correspondence with the general character of the measurements and is intended to make a representation of a fictitious but realistic high stiffness specimen over an interval as large as possible.

The minimum quasi-envelope is fitted to the lowest strength specimens. Five specimens are clearly separated from the rest forming a narrow branch (Fig. 5b). The unconstrained solution (dotted line) gives a very good approximation in a common interval with an undesirable hardening beyond. Therefore, in the constrained solution, the curve is fitted to the end point of the longest set in addition to the usual constraint on the compliances. As these data sets have only a slight curvature, the solution is quite ill-defined with unwanted triple curvature, negative start slope and softening compression range. They can be avoided by introducing constraints for the second derivative at both ends of the compression range. The shape of the solution (solid thick line) is in correspondence with the character of most specimens. The curve truncated at stretch ratio 2.342 (i.e., close to the end) features a compliance matching the entire female sample exactly, thus, the constrained solution is regarded reliable for the entire domain.

Finally, curves are fitted to the data to represent the entire female sample (Fig. 4b). The shortest data set is very short (ending at approx. 1.25), so the unconstrained solution (dotted line) is ill-defined beyond the common interval and has a decreasing unstable section just as in the case of the male subgroup. However, it is robust within the interval so it is again expedient to fit the constrained solution to the end point. In order to control the rest of the fitted curve, the end point is fitted to the mean of four data sets with high strain capacity in the upper right perimeter of the plot. As the range is very large, such constraints are not sufficient to eliminate alternating stable and unstable parts as well as inadequate compression behaviour, therefore, again zero second derivatives are enforced at the start and at the end of the curve. The constrained solution now (solid thick lines) is in accordance with our expectations, i.e., a gentle start followed by hardening and ending in a softening section keeping stability throughout. The *t*-tests show that the compliance of the curve evaluated up to stretch ratio 1.606 is equal to the mean of the entire female sample but the solution can be regarded reliable based on the applied constraints and its appropriate shape.

3. Results

The constants of the Mooney–Rivlin Ψ function of the fitted curves in all six cases being investigated in the previous section are presented in Table 1 together with the upper limit of the unconstrained curve, the minimum and maximum stretch ratio of applicability of the presented constrained models, and the median. Curves beyond the range may significantly diverge from the expected characteristics, and, therefore, application in simulations over the limit is not advised. The curves are plotted in Figs. 3, 4 and 5. Note that though all values of c_{01} in the table are zero, which is not associated with any degenerate behaviour or special case limiting the applicability of the solution in any way, but are in fact due to the conditions on inflexions applied in all cases to produce the mechanically correct shapes both in tension and compression.

Table 1. Constants of 5-parameter Mooney–Rivlin models for all six subsamples: representations for the average and the minimum and maximum quasi-envelopes for both male and female specimens, all values in units of kPa, and stretch range of applicability (minimum, maximum, median, and upper limit of the unconstrained optimization)

Curve fitting	c_{10} [kPa]	c_{01} [kPa]	c_{20} [kPa]	c_{11} [kPa]	c_{02} [kPa]	Min	Limit	Med	Max
Male average	35.535	0.000	514.722	–1876.046	1811.361	0.4	1.250	1.529	1.797
Male minimum quasi-envelope	9.403	0.000	–0.325	4.199	–1.359	0.4	2.053	2.053	2.053
Male maximum quasi-envelope	21.865	0.000	–115.313	–1552.346	2972.482	0.4	1.529	1.556	1.560
Female average	30.569	0.000	136.811	–604.305	705.512	0.4	1.255	1.667	2.248
Female minimum quasi-envelope	6.842	0.000	–5.489	17.781	–5.272	0.4	2.000	2.118	2.600
Female maximum quasi-envelope	183.199	0.000	1185.223	–4167.974	3746.610	0.4	1.421	1.469	1.786

4. Discussion

The five-parameter Mooney–Rivlin curves fitted to data for the representation of the average, minimum and maximum of the stress–stretch ratio curves for male and female specimens are shown together in Figs. 6a and 6b, respectively, plotted over the measurement data with extension to the compression range. In each task it has been shown that the unconstrained solution based on the sum of squared residuals is justified only in the common interval of data and completely invalid beyond, not surprisingly, as it is not bound to any data there. The constrained optimization procedure provided curve fitting for the entire range with specific constraints (related to, e.g., stress, its derivatives, compliance, etc.) chosen in each case as detailed in Section 2. The major difficulty arises from the double characteristics of the data. On one hand, the measurement data are very specific as they come from a number of individuals, but, on the other hand, the mechanical behaviour follows a clear recognizable pattern [11], i.e., combining a gentle start slope with hardening followed by a shorter softening phase in most cases, as is in fact exhibited by most of the specimens. The former feature demanded the constraints to be tailored to the specifics of the given task whereas the latter posed a challenge as to how to produce desirable shape characteristics with algebraic formulation. An additional requirement on energetic stability had to be ensured not only in the tension range of the measurements but in the compression range as well for increased applicability. It was found that wherever constraints for the compression range had to be introduced, they had conveniently negligible effect on the tension zone, without conflicting with other expectation. However, it is a general observation in all cases that the 5-parameter function enables sufficiently flexible curve fitting but tends to produce undesirable fluctuating wavy shape when improperly constrained. It can be noted that the same set of constraints cannot suit every investigated task, instead they were specifically and carefully chosen in each case to capture as much of the explicit numerical characteristics of the data as possible while the expected shape is also achieved.

The unconstrained solution highlights the fact that fitting by least squares only yields extremely ill-defined curves. The interval is effectively technical since λ_{lim} is the ultimate stretch ratio of the single "weakest" specimen in the sample. This single specimen is not representative of the entire sample so we cannot associate it with any mechanical properties. The least squares method is fully justified only up to this limit. Extension of the interval for the entire range is neither justified mathematically nor successful: trial computations showed that the solutions lack any observed mechanical qualities (shape, stability, etc) reported by, e.g., [11]. More sophisticated curve fitting methods, such as the Levenberg–Marquardt algorithm are also of no use, as the Mooney–Rivlin function is linear in its parameters. In fact, the problem itself is not whether or not the curve smoothing methods are sophisticated or fast enough but that they are not applicable for multiple data sets of different lengths (it is because the data sets terminate at different positions and thus data points cannot be taken at equal weights). Any purely mathematical method lacks the mechanical content and, therefore, cannot provide biomechanically correct shapes. The proposed optimization method can overcome this difficulty by applying constraints based on mechanical considerations. In this method, the constraints are correctly enforced (satisfied) and the computational demand is not significant (few tens of seconds). The inadequacy of pure least squares method can be illustrated by the male sample

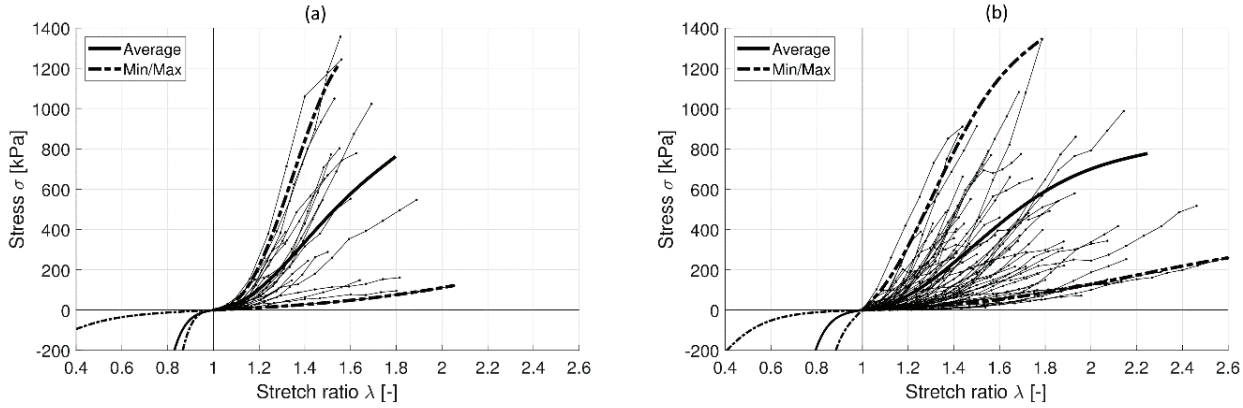

Fig. 6. Simulated curves for male (a) and female specimens (b); measurements are plotted in thin lines with dot markers, average and quasi-envelope solutions are plotted in thick solid and dashed lines, respectively

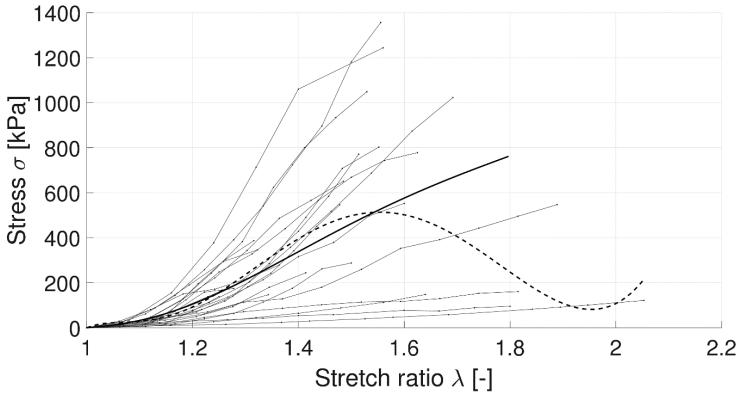

Fig. 7. Comparison of constrained solution and unconstrained least square solution for the entire domain in the male sample: constrained solution (solid thick line) as in Fig. 4(a); unconstrained solution (dashed line) contradicts expected mechanically correct shape in terms of alternating sections, stability, and adequacy even in the initial range

(Fig. 7) where the solid thick curve is the constrained solution given in Fig. 4a, and the dashed line shows the least squares fitting over the entire domain without any constraints. The latter one clearly contradicts the observed shape of stress–strain behaviour [11] in several ways: it has several alternating hardening and softening phases, it is unstable, and gives an unrealistic shape even in the initial range.

5. Conclusions

Following uniaxial tension tests performed on human brain artery walls extracted from aneurysms in a previous research project, in this study, the data have been processed to create stress–stretch curves for the 5-parameter Mooney–Rivlin material model. It is an optimal choice for our purpose as it is flexible enough to obtain biomechanically realistic curves fitting to data over a long range, yet can be controlled by suitable mechanical constraints. The approach proposed hereby combines sum of squared residuals with hard constraints following the Karush–Kuhn–Tucker optimality criteria. We note that several other constitutive models have been proposed for rubber-like materials [4], [7], [9], [11], [37], [45], [47], which can be incorporated in our method with some modification of the solver.

Stress–stretch ratio curves obtained in this work are directly applicable in fluid–solid interaction numerical simulations of aneurysms to support medical treatment, as the model parameters can be readily used in software, the curves cover both compression and tension ranges, and stability of the curves is ensured in the entire range. The results of selections of specimens for extreme soft and stiff as well as the average behaviour separately for both sexes enable numerical simulation and evaluation of expected response of the tissue (note that patient-specific data are impossible to acquire prior to surgery, measurements on specimens from past operations can only be used to generate curves representing collections of specimens).

It was also found that despite the observable differences of stretch and strength capacities between the sexes, male and female samples represented almost identical mean compliance, i.e., strain energy capacity. With possible future expansion of the database by new measurements, this assumption is expected to get further verification and a more refined classification of the sample may also become possible, as well as the solutions can be re-evaluated.

Acknowledgements

This work was completed in the framework of LIT BRAD (Brain Aneurysm Demonstrator) at Johannes Kepler University at Linz, Austria, led by Univ.-Prof. Dr. med. univ. Andreas Gruber and Univ.-Prof. Dr. Zoltán Major. The authors are grateful for the assistance and support provided by the late Prof. Dr. Emil Monos and Dr. Gábor Raffai for launching the experiment series at the Institute of Human Physiology and Clinical Experimental Research of the Semmelweis University, Hungary. The authors thank the team of Prof. Dr. István Nyáry, director at the time at National Institute of Clinical Neurosciences, Budapest, Hungary, for providing samples from surgery.

References

[1] BAZARAA M.S., SHERALI H.D., SHETTY C.M., *Nonlinear Optimization Theory and Algorithms*, John Wiley & Sons, New York, NY, USA, 1993.

[2] BAZILEVS Y., CALO V.M., ZHANG Y., HUGHES T.J.R., *Isogeometric fluid–structure interaction analysis with applications to arterial blood flow*, Comput. Mech., 2006, 38, 310–322, DOI: 10.1007/s00466-006-0084-3.

[3] BENRA F.-K., DOHMEN H.J., PEI J., SCHUSTER S., WAN B., *A Comparison of One-Way and Two-Way Coupling Methods for Numerical Analysis of Fluid-Structure Interactions*, J. Appl. Math., 2011, Article ID 853560, 16 pp., DOI: 10.1155/2011/853560.

[4] CHUONG C.J., FUNG Y.C., *Three-dimensional stress distribution in arteries*, J. Biomech. Eng., 1983, 105 (3), 268–274. DOI: 10.1115/1.3138417.

[5] COSENTINO F., AGNESE V., RAFFA G.M., GENTILE G., BELLAVIA D., ZINGALES M., PILATO M., PASTA S., *The role of material properties in ascending thoracic aortic aneurysms*, Comput. Biol. Med., 2019, 109, 70–78, DOI: 10.1016/j.compbiomed.2019.04.022.

[6] DELFINO A., *Analysis of stress field in a model of the human carotid bifurcation*, Swiss Federal Institute of Technology Lausanne, 1996, DOI: 10.5075/epfl-thesis-1599.

[7] DELFINO A., STERGIOPULOS N., MOORE J.E., MEISTER J.J., *Residual strain effects on the stress field in a thick wall finite element model of the human carotid bifurcation*, J. Biomech., 1997, 30, 777–786, DOI: 10.1016/S0021-9290(97)00025-0.

[8] FUNG Y.C., *Biomechanics: Mechanical Properties of Living Tissues*, Springer-Verlag, New York 1993.

[9] FUNG Y.C., FRONEK K., PATITUCCI P., *Pseudoelasticity of arteries and the choice of its mathematical expression*, Am. J. Physiol. – Heart C., 1979, 237, H620–H631. DOI: 10.1152/ajpheart.1979.237.5.H620.

[10] HOLZAPFEL G.A., *Determination of material models for arterial walls from uniaxial extension tests and histological structure*, J. Theor. Biol., 2006, 238, 290–302. DOI: 10.1016/j.jtbi.2005.05.006.

[11] HOLZAPFEL G.A., GASSER T.C., OGDEN R.W., *A new constitutive framework for arterial wall mechanics and a comparative study of material models*, J. Elasticity, 2000, 61, 1–48, DOI: 10.1023/A:1010835316564.

[12] HOLZAPFEL G.A., OGDEN R.W., *Constitutive modelling of arteries*, P. Roy. Soc. A – Math. Phy., 2010, 466, 1551–1597, DOI: 10.1098/rspa.2010.0058.

[13] HOLZAPFEL G.A., SOMMER G., GASSER C.T., REGITNIG P., *Determination of layer-specific mechanical properties of human coronary arteries with nonatherosclerotic intimal thickening and related constitutive modeling*, Am. J. Physiol. – Heart C., 2005, 289, H2048–H2058. DOI: 10.1152/ajpheart.00934.2004.

[14] HOLZAPFEL G.A., WEIZSÄCKER H.W., *Biomechanical behavior of the arterial wall and its numerical characterization*, Comput. Biol. Med., 1998, 28, 377–392. DOI: 10.1016/S0010-4825(98)00022-5.

[15] HORVATH T., OSZTOVITS J., PINTÉR A. et al., *Genetic impact dominates over environmental effects in development of carotid artery stiffness: a twin study*, Hypertens. Res., 2014, 37, 88–93. DOI:10.1038/hr.2013.133.

[16] HORVATH T., PINTER A., KOLLAI M., *Carotid artery stiffness is not related to endothelial function in young healthy subjects*, Auton. Neurosci., 2012, 166, 85–88, DOI: 10.1016/j.autneu.2011.09.004.

[17] HOU G., WANG J., LAYTON A., *Numerical Methods for Fluid – Structure Interaction – A Review*, Commun. Comput. Phys., 2012, 12, 2, 337–377, DOI: 10.4208/cicp.291210.290411s.

[18] HUDETZ A.G., MONOS E., *A viscoelastic model of mechanically induced and spontaneous contractions of vascular smooth muscle*. Acta Physiol. Hung., 1985, 65, 109–123, pmid:3984755.

[19] KARUSH W., *Minima of functions of several variables with inequalities as side conditions*, M.Sc. dissertation, Department of Mathematics, University of Chicago, 1939.

[20] KOBIELARZ M., JANKOWSKI L.J., *Experimental characterization of the mechanical properties of the abdominal aortic aneurysm wall under uniaxial tension*, J. Theor. App. Mech.–Pol., 2013, 51 (4), 949–958.

[21] KUHN H.W., TUCKER A.W., *Nonlinear programming*, [in:] J. Neyman (Ed.), *Proceedings of Second Berkeley Symposium on Mathematical Statistics and Probability*, University of California Press, 1951, 481–492.

[22] LÁSZLÓ A., PINTÉR A., HORVÁTH T. et al., *Impaired carotid artery elastic function in patients with tetralogy of Fallot*, Heart Vessels, 2011, 26, 542–548, DOI: 10.1007/s00380-010-0095-z.

[23] LAURENCE D.W., HOMBURG H., YAN F. et al., *A pilot study on biaxial mechanical, collagen microstructural, and morphological characterizations of a resected human intracranial aneurysm tissue*, Sci. Rep.-UK, 2021, 11, 3525, DOI: 10.1038/s41598-021-82991-x.

[24] MING-CHEN H., KAMENSKY D., BAZILEVS Y., SACKS M.S., HUGHES T.J.R., *Fluid–structure interaction analysis of bioprosthetic heart valves: significance of arterial wall deformation*, Comput. Mech., 2014, 54, 1055–1071. DOI: 10.1007/s00466-014-1059-4.

[25] MONOS E., *A nagy artériák biomechanikai tulajdonságai. Génsebészet, biomechanika, ökológia*. (9) *A biológia aktuális problémái* (*Biomechanical properties of large arteries. Genetic surgery, biomechanics, ecology*. (9) *Actual problems in biology*), Medicina Könyvkiadó, Budapest 1977 (in Hungarian).

[26] MONOS E., SZŰCS B., *Optimization of hemodynamic energy expenditure in the arterial system*, Obes. Res., 1995, 3, 811S–818S, DOI: 10.1002/j.1550-8528.1995.tb00504.x (Invited review).

[27] MOONEY M., *A theory of large elastic deformation*, J. Appl. Phys., 1940, 11, 582–592, DOI: 10.1063/1.1712836.

[28] MOREL S., KAROL A., GRAF V. et al., *Sex-related differences in wall remodeling and intraluminal thrombus resolution in a rat saccular aneurysm model*, J. Neurosurg., 2021, 134, 58–71, DOI: 10.3171/2019.9.JNS191466.

[29] NOBLE C., CARLSON K.D., NEUMANN E., DRAGOMIR-DAESCU D., ERDEMIR A., LERMAN A., YOUNG M., *Patient specific characterization of artery and plaque material properties in peripheral artery disease*, J. Mech. Behav. Biomed., 2020, 101, 103453, DOI: 10.1016/j.jmbbm.2019.103453.

[30] OGDEN R.W., *Nearly isochoric elastic deformations: application to rubberlike solids*, J. Mech. Phys. Solids, 1978, 26, 37–57.

[31] OGDEN R.W., SCHULZE-BAUER C.A.J., *Phenomenological and structural aspects of the mechanical response of arteries*, [in:] J. Casey, G. Bao (Eds.), *Mechanics in Biology*, The American Society of Mechanical Engineers, 2000, Vol. AMD–Vol. 242/BED–Vol. 46, 125–140,.

[32] PRENDERGAST P.J., LALLY C., DALY S., REID A.J., LEE T.C., QUINN D., DOLAN F., *Analysis of prolapse in cardiovascular stents: a constitutive equation for vascular tissue and finite-element modelling*, J. Biomech. Eng. – T. ASME, 2003, 125, 692–699, DOI: 10.1115/1.1613674.

[33] RHODIN J.A.G., *Architecture of the vessel wall*, [in:] H.V. Sparks, Jr., D.F. Bohr, A.D. Somlyo, S.R. Geiger (Eds.), *Handbook of Physiology*, *The Cardiovascular System*, American Physiologial Society, 1980, Vol. 2, 1–31.

[34] RIVLIN R.S., *Large elastic deformations of isotropic materials. IV. Further developments of the general theory*, Philos. T. Roy. Soc. A, 1948, 241, 379–397, DOI: 10.1098/rsta.1948.0024.

[35] SILVER F.H., CHRISTIANSEN D.L., BUNTIN C.M., *Mechanical properties of the aorta: a review*, Crit. Rev. Biomed. Eng., 1989, 17, 323–358, pmid:2676341.

[36] SKOWRONEK R., KOBEK M., JANKOWSKI Z. et al., *Traumatic basal subarachnoid haemorrhage or ruptured brain aneurysm in 16-year-old boy? – case report*. Archiwum Medycyny Sądowej i Kryminologii (Archives of Forensic Medicine and Criminology), 2016, 66 (1), 32–40. DOI: 10.5114/amsik.2016.62333.

[37] TAKAMIZAWA K., HAYASHI K., *Strain energy density function and uniform strain hypothesis for arterial mechanics*, J. Biomech., 1987, 20, 7–17, DOI: 10.1016/0021-9290(87)90262-4.

[38] TANG A.M., BAKHSHESHIAN J., DING L. et al., *Nonindex Readmission After Ruptured Brain Aneurysm Treatment Is Associated with Higher Morbidity and Repeat Readmission*, World Neurosurg., 2019, 130, e753-e759, DOI: https://doi.org/10.1016/j.wneu.2019.06.214.

[39] TEZDUYAR T.E., SATHE S., SCHWAAB M., CONKLIN B.S., *Arterial fluid mechanics modeling with the stabilized space–time fluid–structure interaction technique*, Int. J. Numer. Meth. Fluids, 2008, 57, 601–629, DOI: 10.1002/fld.1633.

[40] TORII R., OSHIMA M., KOBAYASHI T., TAKAGI K., TEZDUYAR T.E., *Fluid–structure interaction modeling of blood flow and cerebral aneurysm: Significance of artery and aneurysm shapes*, Comput. Methods Appl. Mech. Eng., 2009, 198, 3613–3621, DOI: 10.1016/j.cma.2008.08.020.

[41] TÓTH B., *A vérben áramló vörösvértestek és az érfal mechanikai kölcsönhatása* (*Analysis of the mechanical interaction between the red blood cells and the blood vessels*), PhD dissertation, Budapest University of Technology and Economics, 2011 (in Hungarian).

[42] TÓTH M., NÁDASY G., NYÁRY I., KERÉNYI T., MONOS E., *Agyi aneurizmás betegek intra- és extracranialis artériáinak biomechanikai tulajdonságai* (*Biomechanical properties of intracranialis and extracranialis arteries of brain aneurysm patients*), Érbetegségek, 1996, 3, 1–8 (in Hungarian).

[43] TÓTH M., NÁDASY G., NYÁRY I., KERÉNYI T., OROSZ M., MOLNÁRKA G., MONOS E., *A humán agyi aneurizmazsákok sztérikusan inhomogén viszkoelasztikus viselkedése* (*Steric inhomogeneous viscoelastic behaviour of brain aneurysms*), Érbetegségek, 1997, 4, 1–12 (in Hungarian).

[44] UPADHYAY K., SUBHASH G., SPEAROT D., *Thermodynamics-based stability criteria for constitutive equations of isotropic hyperelastic solids*, J. Mech. Phys. Solids, 2019, 124, 115–142, DOI: 10.1016/j.jmps.2018.09.038.

[45] VAISHNAV R.N., YOUNG J.T., PATEL D.J., *Distribution of stresses and of strain-energy density through the wall thickness in a canine aortic segment*, Circ. Res., 1973, 32, 577–583, DOI: 10.1161/01.RES.32.5.577.

[46] YANG C., BACH R.G., ZHENG J., NAQA I.E., WOODARD P.K., TENG Z., BILLIAR K., TANG D., *In vivo IVUS-based 3-D fluid–structure interaction models with cyclic bending and anisotropic vessel properties for human atherosclerotic coronary plaque mechanical analysis*, IEEE T. Bio-Med. Eng., 2009, 56, 2420–2428, DOI: 10.1109/TBME.2009.2025658.

[47] YEOH O.H., *Some forms of the strain energy function for rubber*, Rubber Chem. Technol., 1993, 66, 754–771. DOI: 10.5254/1.3538343.